Highly Anisotropic Magnetic Domain Wall Behavior in In-Plane Magnetic Films

Xiaochao Zhou,[1,2] Nicolas Vernier,[2,3,*] Guillaume Agnus,[2] Sylvain Eimer,[2] Weiwei Lin,[1] and Ya Zhai[1,†]
[1]School of Physics and Quantum Information Research Center, Southeast University, 211189 Nanjing, China
[2]Centre de Nanosciences et de Nanotechnologies, CNRS, Université Paris-Saclay, 91120 Palaiseau, France
[3]Laboratoire Lumière, Matière et Interfaces, Université Paris-Saclay, 91405 Orsay, France

(Received 8 May 2020; revised 31 July 2020; accepted 13 October 2020; published 1 December 2020)

We have studied the nucleation of magnetic domains and propagation of magnetic domain walls (DWs) induced by pulsed magnetic field in a ferromagnetic film with in-plane uniaxial anisotropy. In contrast to observed behavior in films with out-of-plane anisotropy, the nucleated domains have a rectangular shape in which a pair of the opposite sides are perfectly linear DWs, while the other pair present zigzags. The field induced propagation of these two DW types are found to be different. The linear ones follow a creep law identical to what is usually observed in out-of-plane films, while the velocity of zigzag DWs depends linearly on the applied field amplitude down to very low field. This unexpected feature can be explained by the shape of the DW, and these results provide first experimental evidence of the applicability of the 1D model in two-dimensional ferromagnetic thin films.

DOI: 10.1103/PhysRevLett.125.237203

Introduction.—The propagation of magnetic domain walls (DWs) has been widely studied for out-of-plane magnetic thin films [1–6]. In such films, the absence of inversion symmetry breaking and related phenomena such as Dzyaloshinskii-Moriya interactions [7–11] result in highly isotropic DW propagation. As a result, when the applied field is sufficient to overcome pinning effects, the shape of magnetic domains is expected to become circular [3,4]. While such issues have been investigated in much detail in perpendicularly magnetized films, surprisingly very few works about DW propagation in in-plane full films have been reported to date. The main difficulty resides in the high DW velocities in such samples which renders their detection difficult with the typical field of view of a longitudinal Kerr effect microscope. With the exception of GaMnAs, for which it has been possible to carry out a detailed study of the field dependence of DW velocity [12], it is generally necessary to infer the velocity from other means, such as measurements of the magnetic relaxation [13] and analyses of the laser spot polarization in nanostructured wires [14]. However, most of these have been limited to the one-dimensional limit of wall propagation as the wall extends across the width of the wire and can be considered as a rigid object along this dimension. This no longer holds in two-dimensional films in which the domain walls can deform, particularly in the vicinity of pinning defects.

The dynamical behavior of domain walls in full in-plane magnetized fields therefore remains relatively unexplored. In particular, open questions include the role of short, high-amplitude field pulses, the processes by which nucleation takes place, how the wall propagates, and the ensuing domain shape. Here, we present a study of the dynamic behavior of DW motion in in-plane magnetic films that go toward addressing some of these issues. Our experimental setup allows field pulses of durations as short as 1 μs and of amplitudes up to 2 mT, making it possible to reach the fast velocity regime. The experimental results are analyzed in the framework of a 1D model.

Samples and experiments.—Sample fabrication and magnetic properties: The results we report have been obtained in films with the composition Si/SiO_2 (few nm)/Ta(2 nm)/CoFeB(30 nm)/Ta(1 nm). The films were grown at 300 K on Si(100) substrates with native oxide (spontaneous oxidation at room temperature) by a high vacuum dc sputtering system. No annealing was performed on the samples, which results in the CoFeB film retaining its amorphous as-grown state, with a roughness of around 1 nm. During the film growth, an in-plane magnetic field of around 1 mT was applied which induces a uniaxial anisotropy in the CoFeB layer. The target material is $Co_{60}Fe_{20}B_{20}$. In order to protect the magnetic layer from oxidation, a Ta layer was sputtered above the magnetic film.

Several preliminary experiments have been performed to determine the magnetic properties of the film. The saturation magnetization M_s was measured by a vibrating sample magnetometer was found to be 9.6×10^5 A m^{-1}. An in-plane Kerr hysteresis loop using longitudinal magneto-optic Kerr effect has enabled us to check the coercive field as well as the anisotropy. The easy axis (EA) and hard axis (HA) have been identified (Fig. 1) by examining the hysteresis loops as a function of the angle between the long edge of sample and the applied magnetic field. The coercive field has been determined to be 0.40 mT along the EA. Moreover, Kerr loops measured along the HA were

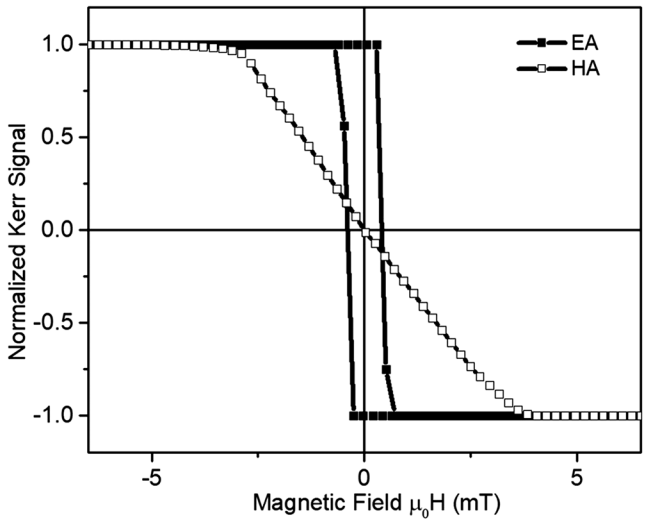

FIG. 1. Kerr hysteresis loops for magnetic in-plane field parallel to easy magnetization axis (EA) and hard magnetization axis (HA).

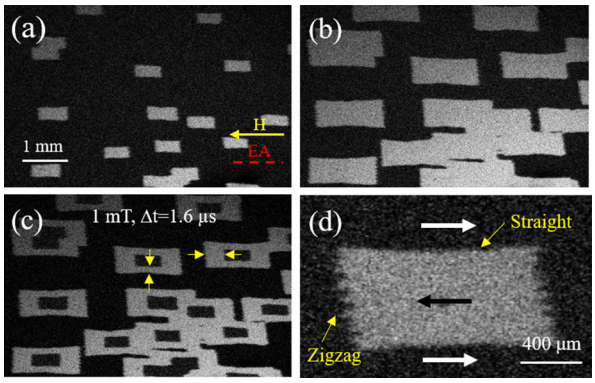

FIG. 2. Typical sequence to measure velocity when the length of the pulsed field is much longer than the rise time. Starting from a saturated state, (a) and (b) show the full-view Kerr images after the application of the (a) first and (b) second pulse field. The pulsed magnetic field (yellow arrow) was parallel to EA (red dash) with amplitude of 1 mT and length of 1.6 μs. (c) shows the DW displacement during the second pulse $\Delta t = 1.6$ μs. (d) presents the magnification of a rectangle domain with two types of DW (horizontal straight and vertical zigzag) being indicated. White (black) arrows denote the magnetization directions outside (inside) the domain.

used to estimate the in-plane magnetic anisotropy (Fig. 1). The shape of the loop is consistent with an anisotropy energy of the form $E_a = -K_a M_s^2 \cos^2\varphi$, where φ is the angle between the magnetization and the EA [15–19], with both directions being in the film plane. The anisotropy field $\mu_0 H_k = 2K_a/M_s$ has been found to be 3.5 mT, which is in agreement with the result of complementary ferromagnetic resonance measurements (see the second part in Supplemental Material [20]) from which we also extracted the Gilbert damping constant $\alpha = 0.0085$ with an error within 5%.

Magnetic domain wall velocity measurements: DW motion was investigated by a longitudinal Kerr microscope at room temperature [21–24]. In this setup, a parallel polarized light beam is directed toward the sample with an incidence angle of 45°, giving rise to a relatively large longitudinal Kerr rotation. The reflected beam was focused on a CMOS camera, where the CMOS sensor plane and the objective were slightly tilted with respect to the beam propagation axis [21,24] so that image plane of the film was in the plane of the sensor. The spatial resolution of this setup is around 30 μm.

The coplanar magnetic pulse field was produced by a small coil of radius 17.5 mm centered on the sample. The field-of-view of the microscope is less than 10 mm, so that the field created by the coil is uniform within a precision of 2% over the area studied. The inductance of the coil is between 4 and 40 μH depending on the coil used, making it possible to create very short field pulses. A high voltage pulse generator was used, so that, with the coil in serial with a resistive charge of 50 Ω, we could obtain current pulses up to 15 A, corresponding to a magnetic field of 2 mT. The fastest rise time with the lowest inductance coil achieved was 83 ns, making it possible to have pulses as short as 1 μs. The sample holder was made of plastic, i.e., an insulating material, so that no eddy currents were induced which can modify the characteristics of the magnetic field generated by the coil. For the work presented here, the magnetic field was always applied along the EA of the sample. DW velocities were measured with the usual stroboscopic approach and Kerr microscopy [1,2,12] (see Supplemental Material [20]).

Results and discussion.—A typical example of DW motion is shown in Fig. 2 in which Fig. 2(a) shows the nucleation and Fig. 2(b) shows the domains after propagation due to the second pulse. Figure 2(c) gives the difference between these two images, which allows the propagation distances to be more easily identified.

The first notable observation concerns the shape of the nucleated domains [Fig. 2(a)], along with their shape after wall propagation [Fig. 2(b)]. In both of these cases, we observe similar highly anisotropic rectangular forms. While minimization of the magnetostatic energy can lead to rectangular domains [24,25], it does not necessarily follow that such shapes remain metastable after wall propagation. In addition, we note that the boundary DW along the horizontal segment is almost straight, while the walls along the vertical boundaries exhibit zigzag structures [Fig. 2(d)]. This again can be explained by static energy minimization [24,26–29]: along the vertical boundaries, because of the in-plane anisotropy, a straight vertical DW would mean head-to-head or tail-to-tail DW (also called charged DW). To avoid the high energetic cost due to this kind of DW, zigzags appear [24,25,30]. Here, we have found that the zigzag angle β of the DW (Fig. 3) does not depend on the

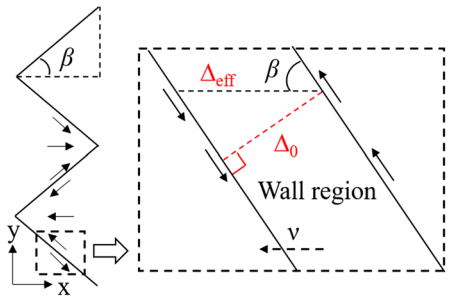

FIG. 3. Left panel: schematic of a zigzag wall as well as the definition of geometrical zigzag angle β; right panel: magnification of a single segment of zigzag wall with the intrinsic DW width Δ_0 and effective DW width Δ_{eff} indicated by red and black dashed lines, respectively. Note that the effective DW width was defined parallel to the propagating direction of the DW marked by dashed arrow.

amplitude of the external pulse field and its value has been found to be approximately 22° (±1.5°), similar to the values found in other samples [30]. This can be explained by assuming some small movements induced by magnetostatic forces after the end of the magnetic pulse, so that β is defined during these movements and is independent of the applied pulse.

The second notable result concerns the velocity, where an asymmetry is seen between the straight, horizontal DW and the zigzag, vertical DW, as shown in Fig. 2(c). The velocities for the two DW types are shown in Fig. 4. First, vertical zigzag DWs go faster than the horizontal straight DW. Second, the corresponding field dependence of the wall velocity is quite different for the two cases: for

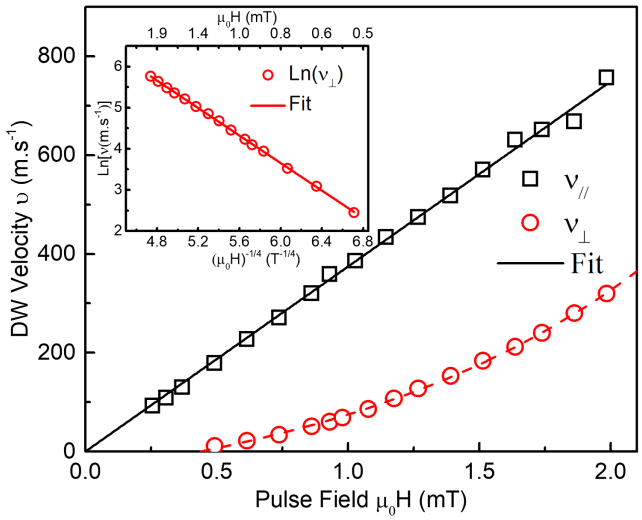

FIG. 4. DW velocity as the function of pulse field for both zigzag and straight wall denoted by $v_{\parallel}$ (black open square) and $v_{\perp}$ (red open circle), respectively. The black solid line is the linear fit with the formula $\nu = \mu$H. The red dashed line is a guide to the eye. The inset shows the plot of Ln(ν) vs $H^{-1/4}$ for the straight wall with the linear fit (red solid line) using Eq. (1).

horizontal straight DWs, we observe motion in the creep regime, which is usually observed in out-of-plane thin films and is described by the relationship [1,2]

$$v(H) = v_0 \exp\left[\left(\frac{H_p}{H}\right)^{1/4}\right]. \tag{1}$$

The observed velocity range extends over almost 2 orders of magnitude. In general, pinning sites are commonly observed in magnetic films, so it is not surprising to recover such behavior in in-plane magnetized films. However, the behavior is quite different for the zigzag DW, where a linear velocity versus field relationship is found where remarkably the intersect at zero field is at zero velocity. While such behavior is consistent with the 1D model [31], it is incompatible with the presence of pinning effects which would result in a finite pinning field for wall displacement.

Analysis.—Below the Walker transition, the one-dimensional wall model predicts the following linear dependence of the wall velocity as a function of applied field:

$$v(H) = \frac{\gamma \mu_0 H \Delta}{\alpha}, \tag{2}$$

where α is the Gilbert damping parameter, γ the gyromagnetic ratio, μ_0 the vacuum permittivity, H the applied field, and Δ the width of the DW, assuming a spatial profile of the form [31,32],

$$\varphi = 2 \arctan\left[\exp\left(\frac{x - x_0}{\Delta}\right)\right]. \tag{3}$$

Based on these relations, we can extract the wall width Δ from the experimental data. From a linear fit of the curve in Fig. 4, we find $\Delta = 17$ nm, which gives a domain wall width of $\pi\Delta = 53$ nm. This value is relatively small for an in-plane magnetized film, but it is of the right order of magnitude [24,25], since other authors have also reported such narrow walls [14] and the nature of the DW can be difficult to ascertain [24,25]. We therefore consider this value as an "effective" width and this is one more point for the validity of 1D model. Let us note that we have not been able to view the Walker breakdown: using the threshold $\alpha M_s/2$ of bulk material [31], we have found a typical value of 6 mT. Because our sample was a thin layer, in which the DW's driving field is more complicated to evaluate, the Walker breakdown might be different [33]. However, from this estimated value, we can think we did not reach the critical Walker value.

Now, the question is why does the 1D model apply for zigzag DW when it obviously does not for horizontal straight DW? A possible explanation is that zigzag is a way of inhibiting the pinning defect effect. Indeed, if the DW meets a pinning defect, it can stay pinned at the very position of the defect while it keeps on moving on its sides.

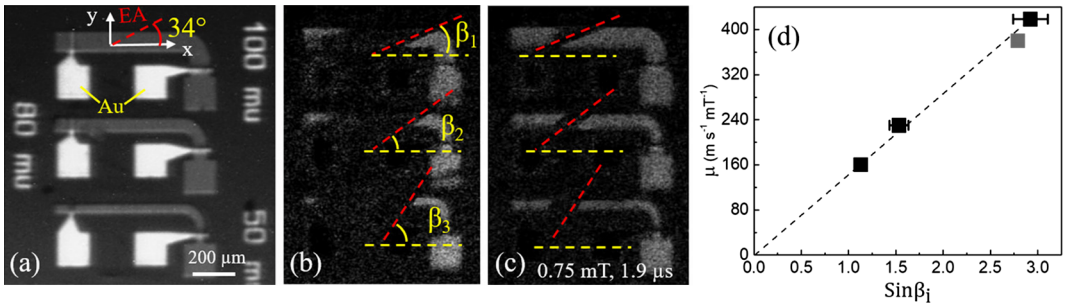

FIG. 5. (a) An optical image of the L-shaped microwires of Ta(2 nm)/CoFeB(30 nm)/Ta(1 nm) stack with wire width of 100, 80, and 50 μm (from top to bottom). The EA has been marked by a red dashed line. The white parts are Au electrodes deposited on the top of the wires (not used in this work). (b) The initial DWs state in which DWs with the "slant" angle β_1, β_2, and β_3 nucleated with a certain pulse in 100, 80, and 50 μm wires, respectively. (c) A typical Kerr image of DWs in the wires after the application of a field pulse with an amplitude of 0.75 mT and length of 1.9 μs. (d) The measured DW mobility μ as the function of $1/\sin\beta$ for the three slant DWs in the wires. Error bar represents the standard deviation of the slant angle in the repeated experiments. The DW mobility for zigzag wall measured in the full film has also been displayed by the red solid square.

As a result, a quite big V shape can be created. In this case, the sizes of the successive zigzags are defined by the defects and the zigzag pattern becomes highly irregular (see Supplemental Material [20], Fig. S5). But, this is true only at low field. Above a threshold field, pinning points become negligible, which means that the zigzag pattern can roughly get back to the regular figure defined by magnetostatic forces (here, the threshold would be around 0.7 mT).

Now, a last question is how should we measure Δ? Indeed, for the horizontal straight DW, the width seems obvious, but the vertical zigzag ones? Should we use Δ_{eff} or Δ (see Fig. 3)? When calculating the velocity, one assumes $\varphi[x - x_0(t)]$, where φ is the tilt angle of the local magnetization, going from 0° to 180° along the wall and x_0 the position of the wall [25,31]. Through this method, the propagation velocity $v = dx_0/dt$ is linked to $\partial\varphi/\partial t$ through $\partial\varphi/\partial t = -v d\varphi/dx$. As $d\varphi/dx$ is proportional to $1/\Delta_{\text{eff}} = \sin\beta/\Delta_0$, we expect DW velocity to be proportional to $\Delta_0/\sin\beta$, where Δ_0 is the "intrinsic width" measured perpendicularly to the DW direction.

Note that the x axis can be chosen in any direction, it does not matter: for an infinite straight DW, the final result is the same. Indeed, if you translate such a DW over $\Delta_0/\sin\beta$ in the x direction, whatever is the x direction, starting from the same initial position, one gets the same final position (see Fig. 3).

To check the $\Delta_0/\sin\beta$ dependency, using optical lithography and ion beam etching (see Supplemental Material [20] for details), we have patterned wires from one of our 30 nm thick CoFeB samples [Fig. 5(a)]. The wires were narrow enough to avoid possible zigzag across their width, but wide enough to ensure that shape anisotropy remains negligible. Several sets of wires with different orientations with respect to the easy axis were patterned to check the effect of the in-plane anisotropy. The variation of the wall velocity was verified at high fields (>1.2 mT), such that pinning is negligible and a 1D behavior according to Eq. (3) could be expected. Figures 5(b) and 5(c) show the nucleation and propagation on one set of wires. Quite surprisingly, the angle β was not the same for all wires and did not appear to depend on the anisotropy axis of the film. This might be due to annealing that is conducted during the patterning process which results in suppressing the EA. As a result, we could plot the mobility $v/\mu_0 H$ as a function of $1/\sin$. As the angle β was reproducible for one wire, it has been possible to perform an average over several experiments in order to get an improved precision. As expected, a clear linear relationship has been obtained which is plotted in Fig. 5(d). In addition, in this graph, we have added a red point that represents the zigzag wall on the full film using the zigzag angle of 22° obtained above. In a wire, shape anisotropy can change K_{eff} and consequently Δ [34]. But, as the wire width is very large, this change is negligible here, and, as expected, this point falls along the trend established by the data for the wires.

Conclusion.—We have found a highly anisotropic dynamical behavior in an in-plane magnetized thin film of Ta/CoFeB/Ta. Using magnetic field pulses parallel to the easy plane, the shape of the domains nucleated by a pulse was rectangular. The limiting DWs of these rectangular domains were different according to the sides. The two sides parallel to the easy magnetization axis were straight lines, while the two sides perpendicular to this axis showed a zigzag structure, as expected from magnetostatics arguments to avoid charged DWs. Depending on the form of the wall, the propagation velocity was very different; creep motion was observed for straight walls, while zigzag walls propagated unimpeded with a linear velocity dependence on applied fields. We suggest that the possibility of creating zigzag at the blocking defects destroys the effect of the pinning. Finally, we have pointed out that the velocity is also changed because of the tilting induced by the zigzag. We have shown that the velocity is proportional to the effective DW width, i.e., the width obtained when

measuring it along the propagation direction. Let us add that some preliminary results with a permalloy film show that the behavior seems to be the same: our results seem typical of in-plane anisotropy thin films with an easy axis in the plane.

This work is supported by the National Key Research and Development Program of China (Grant No. 2017YFA0204800), the National Natural Science Foundation of China (No. 51571062), and the China Scholarship Council. W. L. was supported by the Fundamental Research Funds for the Central Universities (No. 2242020K40105). The authors wish to thank André Thiaville for useful advice, Jian Liang for his experimental support, and Joo-Von Kim for editorial advice.

*Corresponding author.
nicolas.vernier@u-psud.fr
†yazhai@seu.edu.cn

[1] S. Lemerle, J. Ferré, C. Chappert, V. Mathet, T. Giamarchi, and P. Le Doussal, Phys. Rev. Lett. **80**, 849 (1998).
[2] P. J. Metaxas, J. P. Jamet, A. Mougin, M. Cormier, J. Ferré, V. Baltz, B. Rodmacq, B. Dieny, and R. L. Stamps, Phys. Rev. Lett. **99**, 217208 (2007).
[3] K.-W. Moon, J.-C. Lee, S.-G. Je, K.-S. Lee, K.-H. Shin, and S.-B. Choe, Appl. Phys. Express **4**, 043004 (2011).
[4] C. Burrowes, N. Vernier, J.-P. Adam, L. Herrera Diez, K. Garcia, I. Barisic, G. Agnus, S. Eimer, Joo-Von Kim, T. Devolder, A. Lamperti, R. Mantovan, B. Ockert, E. E Fullerton, and D. Ravelosona, Appl. Phys. Lett. **103**, 182401 (2013).
[5] S. Le Gall, N. Vernier, F. Montaigne, M. Gottwald, D. Lacour, M. Hehn, D. Ravelosona, S. Mangin, S. Andrieu, and T. Hauet, Appl. Phys. Lett. **106**, 062406 (2015).
[6] J. Gorchon, S. Bustingorry, J. Ferre, V. Jeudy, and A. B. Kolton, and T. Giamarchi, Phys. Rev. Lett. **113**, 027205 (2014).
[7] E. Jué, A. Thiaville, S. Pizzini, J. Miltat, J. Sampaio, L. D. Buda-Prejbeanu, S. Rohart, J. Vogel, M. Bonfim, O. Boulle, S. Auffret, I. M. Miron, and G. Gaudin, Phys. Rev. B **93**, 014403 (2016).
[8] S.-G. Je, D.-H. Kim, S.-C. Yoo, B.-C. Min, K.-J. Lee, and S.-B. Choe, Phys. Rev. B **88**, 214401 (2013).
[9] R. Soucaille, M. Belmeguenai, J. Torrejon, J.-V. Kim, T. Devolder, Y. Roussigné, S.-M. Chérif, A. A. Stashkevich, M. Hayashi, and J.-P. Adam, Phys. Rev. B **94**, 104431 (2016).
[10] D. Lau, V. Sundar, J.-G. Zhu, and V. Sokalski, Phys. Rev. B **94**, 060401(R) (2016).
[11] K. Shahbazi, J.-V. Kim, H. T. Nembach, J. M. Shaw, A. Bischof, M. D. Rossell, V. Jeudy, T. A. Moore, and C. H. Marrows, Phys. Rev. B **99**, 094409 (2019).
[12] L. Thevenard, S. A. Hussain, H. J. von Bardeleben, M. Bernard, A. Lemaître, and C. Gourdon, Phys. Rev. B **85**, 064419 (2012).
[13] S. Boukari, R. Allenspach, and A. Bischof, Phys. Rev. B **63**, 180402(R) (2001).
[14] G. S. D. Beach, C. Nistor, C. Knutson, M. Tsoi, and J. L. Erskine, Nat. Mater. **4**, 741 (2005).
[15] D. J. Craik, *Magnetism: Principles and Applications* (Wiley-Blackwell, New York, 1995).
[16] J. M. D. Coey, *Magnetism and Magnetic Materials* (Cambridge University Press, Cambridge, England, 2010).
[17] J. Ye, W. He, Q. Wu, H.-L. Liu, X.-Q. Zhang, Z.-Y. Chen, and Z.-H. Cheng, Sci. Rep. **3**, 2148 (2013).
[18] V. W. Guo, B. Lu, X. Wu, G. Ju, B. Valcu, and D. Weller, J. Appl. Phys. **99**, 08E918 (2006).
[19] A. Begué, M. G. Proietti, J. I. Arnaudasa, and M. Ciriaa, J. Magn. Magn. Mater. **498**, 166135 (2020).
[20] See Supplemental Material at http://link.aps.org/supplemental/10.1103/PhysRevLett.125.237203 for experimental details about fabrication, anisotropy measurements through ferromagnetic resonance, magnetic pulse generation, velocity measurements and pinning effects.
[21] J. McCord, J. Phys. D **48**, 333001 (2015).
[22] N. O. Urs, B. Mozooni, P. Mazalski, M. Kustov, Patrick Hayes, S. Deldar, E. Quandt, and J. McCord, AIP Adv. **6**, 055605 (2016).
[23] F. Qiu, G. Tian, J. McCord, J. Zhao, K. Zeng, and P. Hu, AIP Adv. **9**, 015325 (2019).
[24] A. Hubert and R. Schäfer, in *Magnetic Domains* (Springer-Verlag, Berlin, 1998).
[25] A. P. Malozemoff and J. C. Slonczewski, *Magnetic Domain Walls in Bubble Materials* (Academic Press, New York, 1979).
[26] M. J. Freiser, IBM J. Res. Dev. **23**, 330 (1979).
[27] H. Ferrari, V. Bekerisa, and T. H. Johansen, Physica (Amsterdam) **398B**, 476 (2007).
[28] W. Y. Lee, B.-Ch. Choi, Y. B. Xu, and J. A. C. Bland, Phys. Rev. B **60**, 10216 (1999).
[29] B. Cerruti and S. Zapperi, Phys. Rev. B **75**, 064416 (2007).
[30] E. J. Hsieh and R. F. Soohoo, AIP Conf. Proc. **5**, 727 (1972).
[31] N. L. Schryer and L. R. Walker, J. Appl. Phys. **45**, 5406 (1974).
[32] R. C. O'Handley, *Modern Magnetic Materials, Principles and Applications* (Wiley-Interscience Publication, New York, 2000).
[33] A. Mougin, M. Cormier, J. P. Adam, P. J. Metaxas, and J. Ferré, Europhys. Lett. **78**, 57007 (2007).
[34] R. D. McMichael and M. J. Donahue, IEEE Trans. Magn. **33**, 4167 (1997).